Vision-Based, Distributed Control Laws for Motion Coordination of Nonholonomic Robots

Nima Moshtagh*, Nathan Michael*, Ali Jadbabaie*,†, and Kostas Daniilidis*‡

***Abstract*— We study the problem of distributed motion coordination among a group of planar nonholonomic agents. Inspired by social aggregation phenomena such as flocking and schooling in birds and fish, we develop vision-based control laws for parallel and circular formations using a consensus approach. The proposed control laws are distributed, in the sense that only information from neighboring agents are included. Furthermore, the control laws are coordinate-free and do not rely on measurement or communication of heading information among neighbors, but instead require measurements of bearing, optical flow and time-to-collision, all of which can be measured using vision. Collision avoidance capabilities are added to the team members and the effectiveness of the control laws are demonstrated on a group of mobile robots.**

***Index Terms*— Distributed coordination, cooperative control, vision-based control.**

I. Introduction

Cooperative control of multiple autonomous agents has become a vibrant part of robotics and control theory research. The main underlying theme of this line of research is to analyze and/or synthesize spatially distributed control architectures that can be used for motion coordination of large groups of autonomous vehicles. Some of this type of research focus on flocking and formation control [8], [14], [17], [25], [34], synchronization [2], [41], while others focus on rendezvous, distributed coverage and deployment [1], [5]. A key assumption implied in all of the above references is that each vehicle or robot (hereafter called an agent) communicates its position and/or velocity information to its neighbors.

Inspired by the social aggregation phenomena in birds and fish [6], [26], [33], researchers in robotics and control theory have been developing tools, methods and algorithms for distributed motion coordination of multi-vehicle systems. Two main collective motions that are observed in nature are *parallel motion* and *circular motion* [24]. One can interpret stabilizing the circular formation as an example of *activity consensus*, that is, individuals are "moving around" together. Stabilizing the parallel formation is another form of activity consensus in which individuals "move off" together [35].

The circular formation is a circular relative equilibrium in which all the agents travel around the same circle. This kind of behavior is observed in fish schooling, a well studied topic in ecology and evolutionary biology [6]. The *balanced* formation is an interesting family of equilibrium states where the agents are evenly spaced on a circular trajectory, and the geometric center of the agents is fixed. At the equilibrium, the relative headings and the relative distances of the agents determine the shape of the formation [37].

In this paper, we propose a set of control laws for coordinated motions such as parallel and circular formations for a group of planar agents using purely local interactions. The derived control laws are in terms of *shape variables* such as the relative distances and relative headings among the agents. However, these parameters are not readily measurable using simple and basic sensing capabilities. This motivates the rewriting of the derived control laws in terms of biologically measurable parameters. Each agent is assumed to have only monocular vision and capable of measuring basic visual quantities such as *bearing angle*, *optical flow* (bearing derivative) and *time-to-collision*. Rewriting the control inputs in terms of quantities that are locally measurable is equivalent to expressing the inputs in the local body frame. Such a change of coordinate system from global to a local frame provides us with a better intuition on how similar behaviors are carried out in nature.

Verification of the theory through multi-robot experiments demonstrated the effectiveness of the vision-based control laws to achieve different formations. Of course in reality any formation control requires collision avoidance, and indeed collision avoidance cannot be done without range. In order to improve the experimental results, we provided inter-agent collision avoidance properties to the team members. What we show in this paper is that the two tasks of formation-keeping and collision-avoidance can be done with decoupled additive terms in the control law, where the terms for keeping parallel and circular formations depend only on visual parameters.

This paper is organized as follows. In Section II we review a number of important related works. Some background information on graph theory and other mathematical tools used in this paper are provided in Section III. The problem statement is given in Section IV. In Sections VI and V, we derive controllers that stabilize a group of mobile agents into parallel and balanced circular formations, respectively. In Section VII, we present the vision-based controllers that are in terms of the visual measurements among the neighboring agents. In Section VIII, collision avoidance capabilities are added to the control laws. The effectiveness of the proposed controllers are tested on real robots and the experimental results are analyzed in Section IX. The proof of convergence of the controllers can

* The authors are with the GRASP Laboratory, University of Pennsylvania, Philadelphia, PA 19104.
{nima, nmichael, jadbabai, kostas}@grasp.upenn.edu

† Ali Jadbabaie's research is supported in part by the following grants: ARO-MURI W911NF-05-1-0381, ONR/YIP-542371, ONR N000140610436, and NSF-ECS-0347285

‡ Kostas Daniilidis' research is supported in part by: NSF-IIS-0083209, NSF-IIS-0121293, NSF-EIA-0324977, and ARO/MURI DAAD19-02-1-0383.

be found in the Appendices.

II. Related Work And Contributions

The primary contribution of this work is the presentation of simple control laws for achieving parallel and balanced circular formations that only require visual sensing, *i.e.*, the inputs are in terms of quantities that do not require communication among nearest neighbors. In contrast with the work of Paley *et al.* [35], Sepulchre *et al.* [37] and Moshtagh *et al.* [31], where it is assumed that each agent has access to the values of its neighbors' positions and velocities, we design distributed control laws that use only visual clues from nearest neighbors to achieve motion coordination.

Our approach on deriving the vision-based control laws can be classified as an *image-based visual seroving* [13], [43]. In image-based servoing, a number of features are extracted from the image and then the control inputs are computed on the basis of image features directly. In [7], [11], [40] authors use omnidirectional cameras as the only sensor for robots. In In [7], [40] input-output feedback linearization is used to design control laws for leader-following and obstacle avoidance. However, they assume that a specific vertical pose of an omnidirectional camera allows the computation of both bearing and distance. In the work of Mariottini *et al.* [11], the distance measurement is not used, however, the leader uses Extended Kalman filtering to localize its followers and computes the control inputs and guides the formation in a *centralized* fashion. In our work, the control architecture is *distributed*, and we design the formation controllers based on the local interaction among the agents similar to [14] and [25]. Furthermore, for our vision-based controllers no distance measurement is required.

In [29], [36] circular formations of a multi-vehicle system under cyclic pursuit is studied. Their proposed strategy is distributed and relatively simple because each agent needs to measure the relative information from only one other agent. It is also shown that the formation equilibria of the multi-agent system are generalized polygons. In contrast to [29] our control law is a nonlinear function of the bearing angles and as a result our system converges to a different set of stable equilibria.

III. Background

In this section we briefly review a number of important concepts regarding graph theory, regular polygons and Kronecker product that we use throughout this paper.

A. Graph Theory

An (undirected) graph $\mathcal{G}$ consists of a vertex set, $\mathcal{V}$, and an edge set $\mathcal{E}$, where an edge is an unordered pair of distinct vertices in $\mathcal{G}$. If $x, y \in \mathcal{V}$, and $(x, y) \in \mathcal{E}$, then x and y are said to be adjacent, or neighbors and we denote this by writing $x \sim y$. The number of neighbors of each vertex is its valence. A path of length r from vertex x to vertex y is a sequence of $r + 1$ distinct vertices starting with x and ending with y such that consecutive vertices are adjacent. If there is a path between any two vertices of a graph $\mathcal{G}$, then $\mathcal{G}$ is said to be connected.

The adjacency matrix $A(\mathcal{G}) = [a_{ij}]$ of an (undirected) graph $\mathcal{G}$ is a symmetric matrix with rows and columns indexed by the vertices of $\mathcal{G}$, such that $a_{ij} = 1$ if vertex i and vertex j are neighbors and $a_{ij} = 0$, otherwise. We also assume that $a_{ii} = 0$ for all i. The valence matrix, $D(\mathcal{G})$, of a graph $\mathcal{G}$ is a diagonal matrix with rows and columns indexed by $\mathcal{V}$, in which the (i, i)-entry is the valence of vertex i.

The symmetric singular matrix defined as:

$$L(\mathcal{G}) = D(\mathcal{G}) - A(\mathcal{G})$$

is called the Laplacian of $\mathcal{G}$. The Laplacian matrix captures many topological properties of the graph. The Laplacian L is a positive semidefinite M-matrix (a matrix whose off-diagonal entries are all nonpositive) and the algebraic multiplicity of its zero eigenvalue (*i.e.*, the dimension of its kernel) is equal to the number of connected components in the graph. The n-dimensional eigenvector associated with the zero eigenvalue is the vector of ones, $\mathbf{1}_n = [1, \ldots, 1]^T$.

Given an orientation of the edges of a graph, we can define the incidence matrix of the graph to be a matrix B with rows indexed by vertices and columns indexed by edges with entries of 1 representing the source of a directed edge and -1 representing the sink. The Laplacian matrix $L(\mathcal{G})$ of graph $\mathcal{G}$ is represented in terms of its incidence matrix as $L = BB^T$ independent of the orientation of the edges. For more information of graph theory the interested reader is referred to [12].

B. Regular Polygons

Let $d < n$ be a positive integer and define $p = n/d$. Let y_1 be a point on the unit circle. Let R_α be clockwise rotation by the angle $\alpha = 2\pi/p$. The *generalized regular polygon* $\{p\}$ is given by the points $y_{i+1} = R_\alpha y_i$, and edges between points i and $i + 1$ [16].

When $d = 1$ the polygon $\{p\}$ is called an ordinary regular polygon and its edges do not intersect. If $d > 1$ and n and d are coprime, then the edges intersect and the polygon is a *star*. If n and d have a common factor $l > 1$, then the polygon consists of l traversals of the same polygon with $\{n/l\}$ vertices and edges. If $d = n$ the polygon $\{n/n\}$ corresponds to all points at the same location. If $d = n/2$ (with n even), then the polygon consists of two end points and a line between them, with points having an even index on one end and points having an odd index on the other.

C. Kronecker Product

The Kronecker product, denoted by $\otimes$, is an operation on two matrices of arbitrary size resulting in a block matrix. If A is an $m \times n$ matrix and B is a $p \times q$ matrix, then the Kronecker product $A \otimes B$ is a $mp \times nq$ block matrix. If A, B, C and D are matrices of such size that one can form the matrix products AC and BD, then $(A \otimes B)(C \otimes D) = AC \otimes BD$. This is called the mixed-product property. Also the following property holds $(A \otimes B)^T = A^T \otimes B^T$.

IV. Problem Statement

Consider a group of n unit-speed planar agents. Each agent is capable of sensing information from its neighbors. The neighborhood set of agent i, $\mathcal{N}_i$, is the set of agents that can be "seen" by agent i. The precise meaning of "seeing" will be clarified later. The size of the neighborhood depends on the characteristics of the sensors. The neighboring relationship between agents can be conveniently described by a connectivity graph, $\mathcal{G} = (\mathcal{V}, \mathcal{E}, \mathcal{W})$.

Definition 1 (Connectivity Graph): The connectivity graph $\mathcal{G} = (\mathcal{V}, \mathcal{E}, \mathcal{W})$ is a graph consisting of:

- *a set of vertices $\mathcal{V}$ indexed by the set of mobile agents;*
- *a set of edges $\mathcal{E} = \{(i,j) \mid i,j \in \mathcal{V}$, and $i \sim j\}$;*
- *a set of positive edge weights for each edge (i,j).*

The neighborhood of agent i is defined by:

$$\mathcal{N}_i \doteq \{j | i \sim j\} \subseteq \{1, \ldots, n\} \backslash \{i\}.$$

Let us formally define the formations that we are going to consider.

Definition 2 (Parallel Formation): The configuration in which the headings of all agents are the same and velocity vectors are aligned is called the parallel formation.

Note that in the above definition, we do not care about the value of the agreed upon velocity, just the fact that agreement has been reached.

Definition 3 (Balanced Circular Formation): The set of equilibrium states where the agents are evenly spaced on a circular trajectory, and the geometric center of the agents is fixed is called the balanced circular formation.

Let $\mathbf{r}_i$ represent the position of agent i, and $\mathbf{v}_i$ be its velocity vector. The kinematics of each unit-speed agent is given by:

$$\begin{aligned} \dot{\mathbf{r}}_i &= \mathbf{v}_i \\ \dot{\mathbf{v}}_i &= \omega_i \, \mathbf{v}_i^{\perp} \\ \dot{\mathbf{v}}_i^{\perp} &= -\omega_i \mathbf{v}_i \end{aligned} \tag{1}$$

where $\mathbf{v}_i^{\perp}$ is the unit vector perpendicular to the velocity vector $\mathbf{v}_i$. The orthogonal pair $\{\mathbf{v}_i, \mathbf{v}_i^{\perp}\}$ forms a body frame for agent i. We represent the stack vector of all the velocities by $\mathbf{v} = [\mathbf{v}_1^T, \ldots, \mathbf{v}_n^T]^T \in \mathbb{R}^{2n \times 1}$.

The control input for each agent is the angular velocity ω_i. Since it is assumed that the agents move with constant unit speed, the force applied to each agent must be perpendicular to its velocity vector, *i.e.,* the force on each agent is a *gyroscopic force*, and it does not change its speed (and hence its kinetic energy). Thus, ω_i serves as a steering control [17] for each agent. In the following sections we study each formation and design its corresponding distributed control law.

V. Parallel Formations

Our goal in this section is to design a control law for each agent so that the headings of the mobile agents reach an agreement *i.e.,* their velocity vectors are aligned, resulting in a swarm-like pattern. For an arbitrary connectivity graph $\mathcal{G}$, consider the Laplacian matrix $L = BB^T$. We therefore define a measure of misalignment as follows:

$$w(\mathbf{v}) = \frac{1}{2} \sum_{i \sim j} |\mathbf{v}_i - \mathbf{v}_j|^2 = \frac{1}{2} < \mathbf{v}, \bar{L}\mathbf{v} > \tag{2}$$

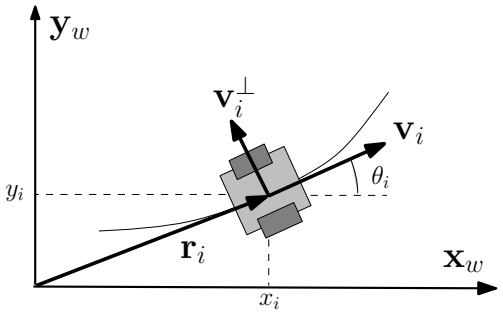

Fig. 1. The trajectory of each agent is represented by a planar Frenet frame.

where the summation is over all the pairs $(i,j) \in \mathcal{E}$, and $\bar{L} = L \otimes I_2 \in \mathbb{R}^{2n \times 2n}$ with I_2 being the 2×2 identity matrix. The time derivative of $w(\mathbf{v})$ is given by

$$\dot{w}(\mathbf{v}) = \sum_{i=1}^{n} < \dot{\mathbf{v}}_i, (\bar{L}\mathbf{v})_i > = \sum_{i=1}^{n} \omega_i < \mathbf{v}_i^{\perp}, (\bar{L}\mathbf{v})_i >$$

where $(\bar{L}\mathbf{v})_i \in \mathbb{R}^2$ is the subvector of $\bar{L}\mathbf{v}$ associated with the i-th agent. Thus, the following gradient control law guarantees that the potential $w(\mathbf{v})$ decreases monotonically:

$$\omega_i = \kappa < \mathbf{v}_i^{\perp}, (\bar{L}\mathbf{v})_i > = -\kappa \sum_{j \in \mathcal{N}_i} < \mathbf{v}_i^{\perp}, \mathbf{v}_{ij} > \tag{3}$$

where $\kappa < 0$ is the gain, and $\mathbf{v}_{ij} = \mathbf{v}_j - \mathbf{v}_i$.

Remark 1: Let θ_i represent the heading of agent i as measured in a fixed world frame (See Figure 1). The unit velocity vector $\mathbf{v}_i$ and its orthogonal vector $\mathbf{v}_i^{\perp}$ are given by: $\mathbf{v}_i = [\cos\theta_i \;\; \sin\theta_i]^T$ and $\mathbf{v}_i^{\perp} = [-\sin\theta_i \;\; \cos\theta_i]^T$. Thus, the control input (3) becomes

$$\omega_i = \kappa \sum_{j \in \mathcal{N}_i} \sin(\theta_i - \theta_j), \;\; \kappa < 0 \; . \tag{4}$$

It is worthwhile to note that the proposed controller is the one used in the synchronization of the Kuramoto model of coupled nonlinear oscillators, which has been extensively studied in mathematical physics as well as control communities [15], [21], [38]. The same model has also been used for phase regulation of cyclic robotic systems [19].

We have the following theorem:

Theorem 1: Consider a system of n unit speed agents with dynamics (1). If the underlying connectivity graph remains fixed and connected, then by applying control input (4) the system converges to the equilibria of $\boldsymbol{\omega} = [\omega_1 \ldots \omega_n]^T = \mathbf{0}$. Furthermore, the velocity consensus set is locally attractive if $\theta_i \in (-\pi/2, \pi/2)$.

Proof: See Appendix XI-A for the proof. ■

Note that $\theta_i \in (-\pi/2, \pi/2) \; \forall i$, is a sufficient condition that restricts the initial headings to a half-circle. The results can be extended to graphs with switching topology as shown in [31].

VI. Balanced Circular Formations

The circular formation is a circular relative equilibrium in which all the agents travel around the same circle. At the equilibrium, the relative headings and the relative distances of the agents determine the shape of the formation. We

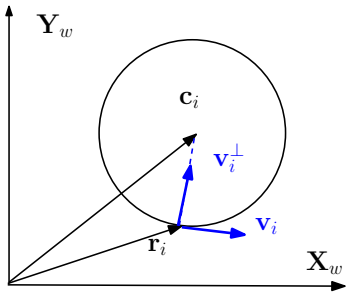

Fig. 2. Center of the circular trajectory is defined as $\mathbf{c}_i = \mathbf{r}_i + (1/\omega_0)\mathbf{v}_i^\perp$.

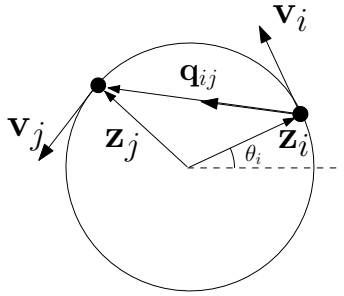

Fig. 3. By a change of coordinate $\mathbf{z}_i = \omega_o(\mathbf{r}_i - \mathbf{c}_i) = -\mathbf{v}_i^\perp$ the problem of generating circular motion in the plane reduces to the problem of balancing the agents on a circle.

are interested in *balanced* circular formations as defined in Definition 3.

Let $\mathbf{c}_i$ represent the position of the center of the i-th circle with radius $1/\omega_o$, as shown in Figure 2, thus

$$\mathbf{c}_i = \mathbf{r}_i + (1/\omega_o)\mathbf{v}_i^\perp \ .$$

The shape controls for driving agents to a circular formation depend on the shape variables $\mathbf{v}_{ij} = \mathbf{v}_j - \mathbf{v}_i$ and $\mathbf{r}_{ij} = \mathbf{r}_j - \mathbf{r}_i$. The relative equilibria of the balanced formation are characterized by $\sum_{i=1}^n \mathbf{v}_i = 0$, and $\mathbf{c}_i = \mathbf{c}_o \in \mathbb{R}^2$ for all $i \in \{1, \ldots, n\}$, where $\mathbf{c}_o$ is the fixed geometric center of the agents.

The control input for each agent has two components:

$$\omega_i = \omega_o + u_i$$

The constant angular velocity ω_o takes the agents into a circular motion, and u_i puts the agents into a balanced formation. In order to design u_i we express the system in a *rotating frame*, which greatly simplifies the analysis. By a change of variable

$$\mathbf{z}_i = \omega_o(\mathbf{r}_i - \mathbf{c}_i) = -\mathbf{v}_i^\perp$$

the problem reduces to balancing the agents on a unit circle as shown in Figure 3. The new coordinate system is rotating with angular velocity ω_o. The dynamics in the rotating frame is given by

$$\begin{aligned} \dot{\mathbf{z}}_i &= \mathbf{v}_i u_i \\ \dot{\mathbf{v}}_i &= -\mathbf{z}_i u_i \ , \quad i = 1, \ldots, n \end{aligned} \tag{5}$$

The new position vector $\mathbf{z}_i$ is a unit vector, however its speed $|\dot{\mathbf{z}}_i|$ is not constant anymore, and it is proportional to u_i, which goes to zero as the group reaches a balanced formation.

Let us define $\mathbf{z}_{ij} = \mathbf{z}_j - \mathbf{z}_i$ and $\mathbf{q}_{ij} = \mathbf{z}_{ij}/|\mathbf{z}_{ij}|$ as the unit vector along the relative position vector $\mathbf{z}_{ij}$. We note that at the balanced equilibrium the velocity of each agent must be perpendicular to $\bar{\mathbf{q}}_i = \sum_{j \in \mathcal{N}_i} \mathbf{q}_{ij}$, which is a vector along the average of the relative position vectors that are incident to agent i. Thus, the quantity $< \mathbf{v}_i, \bar{\mathbf{q}}_i >$ vanishes at the balanced equilibrium. Hence we propose the following control law for the balanced formation:

$$u_i = -\kappa < \mathbf{v}_i, \bar{\mathbf{q}}_i > = -\kappa \sum_{j \in \mathcal{N}_i} < \mathbf{v}_i, \mathbf{q}_{ij} > \quad \kappa > 0 \ . \tag{6}$$

Suppose the underlying connectivity graph is a complete graph. Now we have the following theorem for reaching the balanced circular formation in a group of mobile planar agents with a complete-graph connectivity.

Theorem 2: Consider a system of n agents with kinematics (5). Given a complete connectivity graph $\mathcal{G}$, and applying control law (6), the n-agent system (almost) globally asymptotically converges to a balanced circular formation as defined in Definition 3.

Proof: See Appendix XI-A for the proof. ■

Next we consider the situation that the connectivity graph has a ring topology. We denote this graph with $\mathcal{G}^{ring}$. We have the following theorem for balanced circular formations of mobile agents with ring topology.

Theorem 3: Consider a system of n agents with kinematics (5). Suppose the connectivity graph has the ring topology $\mathcal{G}^{ring}$ and each agent applies the balancing control law (6). Let ϕ_o be the angle to which the relative headings converge. Then if $\phi_o \in (\pi/2, 3\pi/2)$, the balanced equilibrium is locally exponentially stable.

Proof: See Appendix XI-C for the proof. ■

As a result of Theorem 3 at the equilibrium the final configuration for $\mathcal{G}^{ring}$ is either a star polygon (for n odd), or a line (for n even) with odd-indexed agents on one side and even-indexed agents on the other side. This can be seen by noting that for a $\{n/d\}$ polygon, the angle between the connected nodes is $2\pi d/n$. Thus, the stable equilibria given by $\phi_o \in (\pi/2, 3\pi/2)$ correspond to polygons with $d \in (n/4, 3n/4)$. For example, for $n = 5$, the stable polygons are $\{5/3\}$ and $\{5/4\}$ which are the same polygons with reverse ordering of the nodes. Simulations suggest that the largest region of attraction for n even belongs to a polygon $\{n/d\}$ with $d = n/2$, and a *star* polygon $\{n/d\}$ with $d = (n \pm 1)/2$ for n odd. These results are observed in experiments with real robots as demonstrated in Section IX.

VII. Vision-Based Control Laws

Notice that the control inputs (4) and (6) for rectilinear and circular formations depend on the *shape variables*, *i.e.*, relative headings and positions, which are not directly measurable using visual sensors such as a single camera on a robot, because estimation of the relative position and motion requires binocular vision. Thus, we write (4) and (6) in terms of parameters that are entirely measurable using a simple visual sensor.

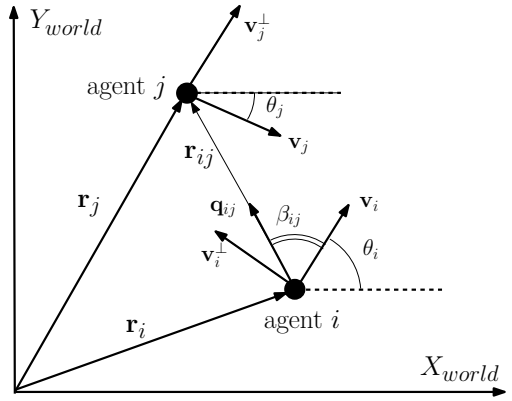

Fig. 4. Bearing angle β_{ij} is measured as the angle between the velocity vector (along body x-axis) and vector $\mathbf{r}_{ij}$, which connects the two neighboring agents.

Let $\mathbf{r}_i = [x_i \; y_i]^T$ be the location of agent i in a fixed world frame, and $\mathbf{v}_i = [\dot{x}_i \; \dot{y}_i]^T$ be its velocity vector. The heading or orientation of agent i is then given by

$$\theta_i = \text{atan2}(\dot{y}_i, \dot{x}_i) \; . \tag{7}$$

With the above definitions and knowing that agents have unit speed, dynamic model (1) becomes the unicycle model:

$$\begin{aligned} \dot{x}_i &= \cos\theta_i \\ \dot{y}_i &= \sin\theta_i \\ \dot{\theta}_i &= \omega_i \end{aligned} \tag{8}$$

where ω_i is the angular velocity of agent i.

Next, we define the visual parameters that we will use later to derive the vision-based control laws. Let β_{ij} be the relative angle between $\mathbf{q}_{ij}$, the projection of agent j in the local coordinate frame of i, and $\mathbf{v}_i$, the velocity of agent i. The bearing angle β_{ij} is defined as (see Figure 4):

$$\beta_{ij} \doteq \text{atan2}(y_i - y_j, x_i - x_j) - \theta_i \; . \tag{9}$$

The rate of change of bearing $\dot{\beta}_{ij}$ is called *optical flow*. One can see from Figure 5 that $\dot{\beta}_{ij}$ (the optical flow corresponding to agent j as seen by agent i) is equal to the projection of the scaled relative velocity vector $\dot{\mathbf{r}}_{ij}/l_{ij}$ perpendicular to the unit bearing vector $\mathbf{q}_{ij} = [\cos\beta_{ij} \;\; \sin\beta_{ij}]^T$. More precisely,

$$\dot{\beta}_{ij} = < \frac{\dot{\mathbf{r}}_{ij}}{l_{ij}}, \mathbf{q}_{ij}^\perp > \tag{10}$$

where $l_{ij} = |\mathbf{r}_{ij}|$. The reader should also note that only one optical flow measurement per rigid body is taken. Thus, making it impossible to rely on structure from motion algorithms. Regarding optical flow, we refer the reader to the survey [3].

Finally time-to-collision, τ_{ij}, can be estimated from the ratio of area change to area or from the divergence of the optical flow [4], [20]. Incidentally, experimental evidence suggests that several animal species, including pigeons and flies, are capable of estimating time-to-collision [9], [22], [42], or the inverse of time-to-collision, also known as *loom* [27]. Actually "loom" is the parameter that we need, and it is given by:

$$\frac{1}{\tau_{ij}} = \frac{\dot{a}_{ij}}{a_{ij}} = \frac{\dot{l}_{ij}}{l_{ij}} = \; < \frac{\dot{\mathbf{r}}_{ij}}{l_{ij}}, \mathbf{q}_{ij} > \; , \tag{11}$$

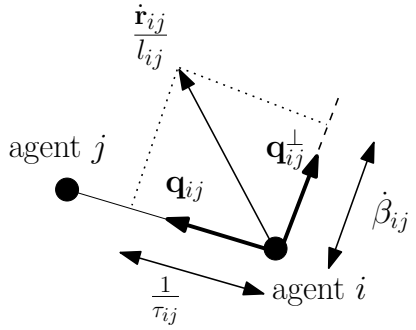

Fig. 5. The optical flow $\dot{\beta}_{ij}$ and loom $1/\tau_{ij}$ can be written in terms of the scaled relative velocity.

where the last equality can be deduced from Figure 5. Note that the measurement of time-to-collision τ_{ij} is not equivalent to the measurement of the relative distance between the agents as is usually the case in visual motion problems. This is due to the fact that time-to-collision can only recover the distance up to an unknown factor which in our case is different for every neighboring agent.

Thus, to formally define sensing, we assume that each agent i can measure:

- β_{ij} as the bearing angle,
- $\dot{\beta}_{ij}$ as the optical flow,
- τ_{ij} as time-to-collision

for any agent j in the set of neighbors $\mathcal{N}_i$. In what follows, we show how to write the control inputs (4) and (6) in terms of the measurable quantities defined above.

A. Parallel Formation

In this section we derive a vision-based control law for parallel motion of a group of nonholonomic agents. The input for parallel motion (4) is in terms of the relative headings. In order to derive the vision-based control law we need to consider the following slightly modified version of the control law given by (4):

$$\omega_i = \sum_{j \in \mathcal{N}_i} \frac{-\kappa}{|\mathbf{r}_{ij}|} < \mathbf{v}_i^\perp, \mathbf{v}_{ij} > = \sum_{j \in \mathcal{N}_i} \frac{\kappa}{l_{ij}} \sin(\theta_i - \theta_j) \tag{12}$$

where $\kappa < 0$, and we have normalized each term in the summation by the relative distance l_{ij} between the agents. The need for the normalization factor $1/l_{ij}$ becomes clear in the derivation of the vision-based control law. It also can be explained by noting that the *normalized* relative velocity vector can be written in terms of the measurable quantities of optical flow (10) and time-to-collision (11) (see Figure 5).

Now we can derive the vision-based control law for the parallel formation that is equivalent to (12). The equation describing the relative motion of agents i and j is given by:

$$\dot{\mathbf{r}}_{ij} = -\boldsymbol{\omega}_i \times \mathbf{r}_{ij} + \mathbf{v}_{ij} \tag{13}$$

where $\boldsymbol{\omega}_i = [0 \; 0 \; \omega_i]^T$ is the body angular velocity vector of agent i, and all the vectors in the above equation are expressed in the body frame of agent i. We normalize the optical flow

equation (13) by dividing it by l_{ij} to get

$$\frac{\dot{\mathbf{r}}_{ij}}{l_{ij}} = -\boldsymbol{\omega}_i \times \mathbf{q}_{ij} + \frac{\mathbf{v}_{ij}}{l_{ij}}, \quad \forall j \in \mathcal{N}_i \tag{14}$$

where $\mathbf{q}_{ij} = \mathbf{r}_{ij}/|\mathbf{r}_{ij}|$. Equation (14) holds for all the agents that are in $\mathcal{N}_i$. Thus, we sum (14) over all $j \in \mathcal{N}_i$ to get:

$$\sum_{j\in\mathcal{N}_i} \frac{\dot{\mathbf{r}}_{ij}}{l_{ij}} = -\sum_{j\in\mathcal{N}_i} \boldsymbol{\omega}_i \times \mathbf{q}_{ij} + \sum_{j\in\mathcal{N}_i} \frac{\mathbf{v}_{ij}}{l_{ij}} \tag{15}$$

Note that all the parameters in (15) are expressed in the body frame of agent i. The goal is to solve (15) for input $\boldsymbol{\omega}_i$ so that it is only a function of some measurable quantities such as bearing and time-to-collision.

Let us use the following notation

$$\mathbf{m}_i = \sum_{j\in\mathcal{N}_i} \frac{\dot{\mathbf{r}}_{ij}}{l_{ij}}, \quad \mathbf{q}_i = \sum_{j\in\mathcal{N}_i} \mathbf{q}_{ij} \ .$$

It is easy to show that $\mathbf{m}_i$ is a measurable vector. When we differentiate $\mathbf{r}_{ij} = l_{ij}\mathbf{q}_{ij}$, we get $\dot{\mathbf{r}}_{ij} = \dot{l}_{ij}\mathbf{q}_{ij} + l_{ij}\dot{\mathbf{q}}_{ij}$. Therefore, we get

$$\mathbf{m}_i = \sum_{j\in\mathcal{N}_i} \frac{\dot{\mathbf{r}}_{ij}}{l_{ij}} = \sum_{j\in\mathcal{N}_i} \left(\frac{\mathbf{q}_{ij}}{\tau_{ij}} + \dot{\mathbf{q}}_{ij}\right) \ . \tag{16}$$

The bearing vector $\mathbf{q}_{ij}$ and the optical flow vector $\dot{\mathbf{q}}_{ij}$ in the body-frame of agent i are given by

$$\mathbf{q}_{ij} = \begin{bmatrix}\cos\beta_{ij}\\ \sin\beta_{ij}\end{bmatrix}, \qquad \dot{\mathbf{q}}_{ij} = \dot{\beta}_{ij}\begin{bmatrix}-\sin\beta_{ij}\\ \cos\beta_{ij}\end{bmatrix} = \dot{\beta}_{ij}\mathbf{q}_{ij}^{\perp} \ .$$

Therefore $\mathbf{m}_i$ is measurable. See Figure 5 for details.

Given that the velocity of agent i is along the x-axis of its body frame, vectors $\mathbf{v}_i$ and $\mathbf{v}_j$ can be expressed in the i-th body frame as

$$\mathbf{v}_i = \begin{bmatrix}1\\0\end{bmatrix} \qquad \mathbf{v}_j = \begin{bmatrix}\cos(\theta_j-\theta_i)\\ \sin(\theta_j-\theta_i)\end{bmatrix} = \begin{bmatrix}\cos(\theta_i-\theta_j)\\ -\sin(\theta_i-\theta_j)\end{bmatrix} \ .$$

By substituting for $\boldsymbol{\omega}_i$ and $\mathbf{v}_{ij}$ in (15) we get:

$$\mathbf{m}_i = -\begin{bmatrix}0 & -\omega_i\\ \omega_i & 0\end{bmatrix}\mathbf{q}_i + \sum_{j\in\mathcal{N}_i}\frac{1}{l_{ij}}\begin{bmatrix}\cos(\theta_i-\theta_j)-1\\ -\sin(\theta_i-\theta_j)\end{bmatrix}.$$

The above relation gives us two sets of linear equations. The second equation is:

$$(\mathbf{m}_i)_y = -\omega_i(\mathbf{q}_i)_x - \sum_{j\in\mathcal{N}_i}\frac{1}{l_{ij}}\sin(\theta_i-\theta_j) \ , \tag{17}$$

where $(\cdot)_x$ and $(\cdot)_y$ are the x and y components of a vector. We can see that the last term on the right is actually the input given by (12) scaled by factor $1/\kappa$. Hence (17) becomes:

$$(\mathbf{m}_i)_y = -\omega_i(\mathbf{q}_i)_x + \frac{1}{\kappa}\omega_i \ ,$$

which can be solve for ω_i. After substituting for $(\mathbf{m}_i)_y$ and $(\mathbf{q}_i)_x$ we get:

$$\omega_i = \frac{-\kappa\sum_{j\in\mathcal{N}_i}\left(\frac{1}{\tau_{ij}}\sin\beta_{ij} + \dot{\beta}_{ij}\cos\beta_{ij}\right)}{1+\kappa\sum_{j\in\mathcal{N}_i}\cos\beta_{ij}}, \ \kappa<0. \tag{18}$$

This is the vision-based control law that is equivalent to (4) and takes a group of kinematic agents to a parallel formation. See Section IX for the experimental verification of the results.

B. Balanced Formation

As we show next, the only visual parameter that is required for generating a balanced circular formation is the *bearing angle*, β_{ij}. It is remarkable that we can generate interesting global patterns using only a single measurement of the bearing angle. Note that the inner product of two vectors is independent from the coordinate system in which they are expressed. Thus, given $\mathbf{v}_i = [1\ 0]^T$ and $\mathbf{q}_{ij} = [\cos\beta_{ij}\ \ \sin\beta_{ij}]^T$ in the body frame of agent i, the control input for balanced circular formation can be written as:

$$\omega_i = \omega_o - \kappa\sum_{j\in\mathcal{N}_i} < \mathbf{v}_i, \mathbf{q}_{ij} > = \omega_o - \kappa\sum_{j\in\mathcal{N}_i}\cos\beta_{ij} \ , \tag{19}$$

where $\kappa > 0$. Input (19) is the desired vision-based control input.

VIII. Formation Control With Collision Avoidance

The central contribution of this work is providing simple vision-based control laws for reaching parallel and balanced circular formations. Of course in reality any formation control requires collision avoidance, and indeed collision avoidance cannot be done without range. What we show here is that the two tasks can be done with decoupled additive terms in the control law, where the term for circular formation depends only on bearing.

To ensure collision avoidance and cohesion of the formation, an inter-agent potential function [32], [39] is defined. A control law from this artificial potential function results in simple steering behaviors known as *separation* and *cohesion* that govern how each agent maneuvers based on the relative position of its neighbors. The global minimum of this function is where all the agents are at the desired distances.

It was shown in [39] that only if the underlying proximity graph is a spanning tree, the formation stabilizes at a state where the potential function is at the global minimum, and all the agents are at the desired distances. Whereas, in the general case, the multi-agent system reaches a stable state where the potential energy of the system is minimized (a local minimum). Next we formally define the notion of potential function used in this paper.

The potential function $f_{ij}(|\mathbf{r}_{ij}|)$ is a symmetric function of the distance $|\mathbf{r}_{ij}| = l_{ij}$ between agents i and j, and is defined as follows [39]:

Definition 4 (Potential Function): Potential f_{ij} is a differentiable, nonnegative function of the distance $|\mathbf{r}_{ij}|$ between agents i and j such that,

- *$f_{ij} \to \infty$ as $|\mathbf{r}_{ij}| \to 0$.*
- *f_{ij} attains its unique minimum when agents i and j are located at a desired distance.*

This definition ensures that minimization of the inter-agent potential functions leads to the desired cohesion and separation in the group. Agent i's total potential is given by

$$f_i = \sum_{j\in\mathcal{N}_i} f_{ij}(|\mathbf{r}_{ij}|) \ . \tag{20}$$

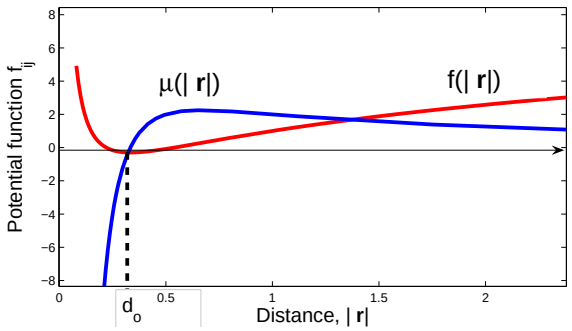

Fig. 6. Artificial potential function f_{ij}, and the norm of its gradient μ_{ij}.

The requirements for f_{ij} given in Definition 4 supports a large class of functions. Similar potential functions as the following are used in both [39] and [18]:

$$f_{ij} = \frac{d_0}{|\mathbf{r}_{ij}|} + \log|\mathbf{r}_{ij}| \ ,$$

where d_0 is the desired distance between the neighboring agents. This choice of f_{ij} provides an *attractive* force when an agent is moving away from the group, and a *repulsive* force when two agents get too close to each other. The gradient of this function is given by

$$\nabla_{\mathbf{r}_{ij}} f_{ij} = \frac{\mathbf{r}_{ij}}{|\mathbf{r}_{ij}|}\left(\frac{1}{|\mathbf{r}_{ij}|} - \frac{d_0}{|\mathbf{r}_{ij}|^2}\right) = \mu(|\mathbf{r}_{ij}|)\mathbf{q}_{ij} = \mu_{ij}\mathbf{q}_{ij}. \tag{21}$$

See Figure 6 for the plots of the potential function f_{ij}, and the norm of its gradient μ_{ij}.

The control inputs for parallel and balanced formations must have an additional components α_i that controls the spacing between the agents. α_i steers the agents to avoid collisions or pull them together if they are separating too far apart. For the inserted force to be gyroscopic, it must be perpendicular to the velocity vector $\mathbf{v}_i$ and along $\mathbf{v}_i^\perp$. The force is proportional to the negative gradient of the potential function f_i. Thus, as a result the spacing control must have the form

$$\alpha_i = -\kappa_p < \mathbf{v}_i^\perp, \nabla_{\mathbf{r}_i} f_i >, \quad \kappa_p > 0 \ . \tag{22}$$

Note that since $\mathbf{r}_{ij} = \mathbf{r}_j - \mathbf{r}_i$ we have

$$\nabla_{\mathbf{r}_i} f_i = -\nabla_{\mathbf{r}_{ij}} f_i = -\sum_{j\in\mathcal{N}_i} \nabla_{\mathbf{r}_{ij}} f_{ij} = -\sum_{j\in\mathcal{N}_i} \mu_{ij}\mathbf{q}_{ij} \ .$$

We have the following theorem for parallel formations with collision avoidance:

Theorem 4 (Parallel Formation): Consider a system of n agents with dynamics (1) and applying the control input

$$\begin{aligned} \omega_i &= u_i + \alpha_i \\ &= \kappa_1 < \mathbf{v}_i^\perp, (\bar{L}\mathbf{v})_i > + \kappa_p < \mathbf{v}_i^\perp, \nabla_{\mathbf{r}_{ij}} f_i > \\ &= -\kappa_1 \sum_{j\in\mathcal{N}_i} < \mathbf{v}_i^\perp, \mathbf{v}_j > + \kappa_p \sum_{j\in\mathcal{N}_i} \mu_{ij} < \mathbf{v}_i^\perp, \mathbf{q}_{ij} > \end{aligned} \tag{23}$$

where $\kappa_1 < 0$, $\kappa_p > 0$. Given that the underlying connectivity graph $\mathcal{G}$ remains connected, all agents locally asymptotically converge to the velocity consensus set, and collisions between the interconnected agents are avoided, and at the equilibrium the potential energy of the n-agent system is minimized.

Proof: See Appendix XI-D for the proof. ■

As it is shown in the proof of Theorem 4, the stable configuration attains the global minimum of the potential function only if the underlying proximity graph is a spanning tree. In such case all the agents are at the desired distances. In the general case, the multi-agent system reaches a stable configuration where the potential energy of the system is minimized (*i.e.,* the system stabilizes at a local minimum of the potential function). Similarly, we have the following proposition for reaching a balanced circular formation with inter-agent collision avoidance:

Proposition 1 (Circular Formation): Consider a system of n agents with dynamics (1) and applying the control input

$$\begin{aligned} \omega_i &= \omega_o + u_i + \alpha_i \\ &= \omega_o - \kappa_1 \sum_{j\in\mathcal{N}_i} < \mathbf{v}_i, \mathbf{q}_{ij} > + \kappa_p \sum_{j\in\mathcal{N}_i} \mu_{ij} < \mathbf{v}_i^\perp, \mathbf{q}_{ij} > \end{aligned} \tag{24}$$

where $\kappa_1 > 0$ and $\kappa_p > 0$. Given that $\mathcal{G}$ remains connected, the n-agent system asymptotically reaches the balanced formation, and collisions between the interconnected agents are avoided.

IX. Experiments

In this section we show the results of experimental tests for balanced circular and parallel formations. But first, let us describe the experimental testbed.

Robots: We use a series of small form-factor robots called *Scarab* [30]. The *Scarab* is a 20 x 13.5 x 22.2 cm^3 indoor ground platform with a mass of $8\ kg$. Each *Scarab* is equipped with a differential drive axle placed at the center of the length of the robot with a 21 cm wheel base (See Figure 7). Each *Scarab* is equipped with an onboard computer, power management system and wireless communication. Each robot is actuated by stepper motors that allows us to model it as a point robot with unicycle kinematics (8) for its velocity range. The linear velocity of each robot is bounded at $0.2\ m/s$. Each robot is able to rotate about its center of mass at speeds below $1.5\ rad/s$. Typical angular velocities resulting from the control law were below $0.5\ rad/s$.

Software: Every robot is running identical modularized software with well defined interfaces connecting modules via

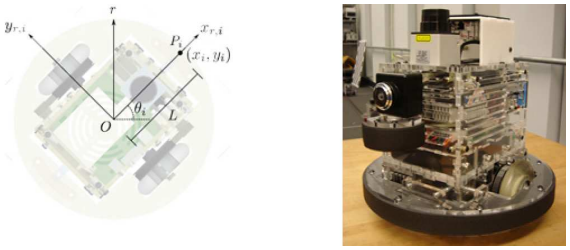

Fig. 7. The *Scarab* is a small robot with a differential drive axle. LED markers are placed on top of each *Scarab* for pose estimation.

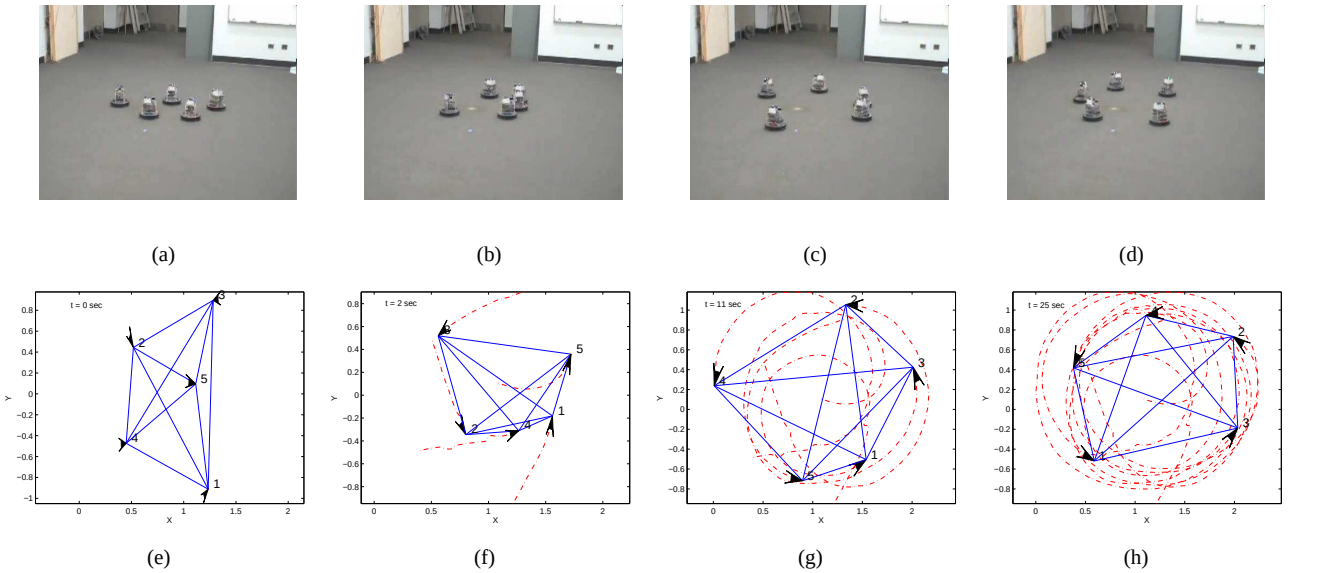

Fig. 8. Five *Scarabs* form a circular formation starting with a complete-graph topology. (a) At time $t = 0$ robots starts at random positions and orientations. (b) $t = 2$ sec. (c) $t = 11$ sec. (d) At $t = 25$ sec. the robots reach a stable balanced configuration around a circle with radius of 1m. Figures (e) through (h) show the actual trajectories of the robots and their connectivity graph at the times specified above. Figure 8(h) shows that the final configuration is a regular polygon.

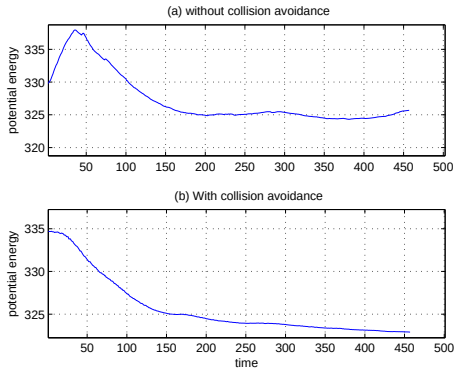

Fig. 9. comparison of the values of the 5-agent system's potential energy while robots are applying (a) control input (19) and (b) control input (24) with collision avoidance.

the *Player* robot architecture system [10], which consists of libraries that provide access to communication and interface functionality. The *Player* also provides a close collaboration with the three-dimensional physics-based simulation environment *Gazebo*. *Gazebo* provides the powerful ability to transition transparently from code running on simulated hardware to real hardware.

Infrastructure: In the experiments, visibility of the robot's set of neighbors is the main issue. Using omnidirectional cameras seems to be a natural solution. However, in order to reduce the on-board computation, a tracking system consisting of LED markers on the robots and eight overhead cameras is designed. This ground-truth verification system can locate and track the robots with position error of approximately $2\ cm$ and an orientation error of 5°. The overhead tracking system allows control algorithms to assume pose is known in a global reference frame. The process and measurement models fuse local odometry information and tracking information from the camera system. Each robot locally estimates its pose based on the globally available tracking system data and local motion, using an extended Kalman filter. We process global overhead tracking information but hide the global state of the system from each robot, providing only the current state of the robot as well as the positions of each robot's set of neighbors. In this way, we use the tracking system in lieu of an inter-robot sensor implementation.

In all the experiments the neighborhood relations, *i.e.*, the connectivity graphs, are fixed and undirected. Each robot computes the visual measurements with respect to its neighbors from equations (9) and (11). The conclusions for each set of experiments are drawn from significant number of successful trials that supported the effectiveness of the designed controllers. The results of the experiments are provided in the following subsections.

A. Circular Motion With Complete-Graph Topology

First we applied the bearing-only control law (19) to a group of $n = 5$ robots without considering collision avoidance among the agents. In Figures 8(a) through 8(d) snapshots from the actual experiment are shown, and in Figures 8(e) through 8(h) the corresponding trajectories, generated from overhead tracking information, are demonstrated. Note that for the complete-graph topology the ordering of the robots in the final configuration is not unique, and it depends on the initial positions.

Since there was no collision avoidance implemented in the experiments of Figure 8 the robots could become undesirably close to one another as it can be seen in Fig. 8(b). However, by applying control input (24) no collisions occur among the robots as they reach the equilibrium. The actual trajectories of $n = 5$ robots for this scenario are shown in Figure 10. The

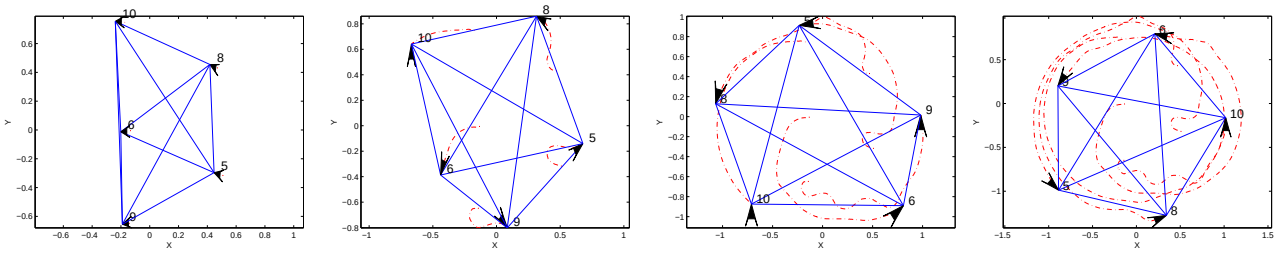

(a) (b) (c) (d)

Fig. 10. Five *Scarabs* form a circular formation starting with a complete-graph topology while avoiding collisions. (a) $t = 0$ sec. (b) $t = 8$ sec. (c) $t = 20$ sec. (d) At $t = 36$ sec. the robots reach a stable balanced configuration around a circle with radius of 1m. Figures (a) through (d) show the actual trajectories of the robots and their connectivity graph at the times specified above.

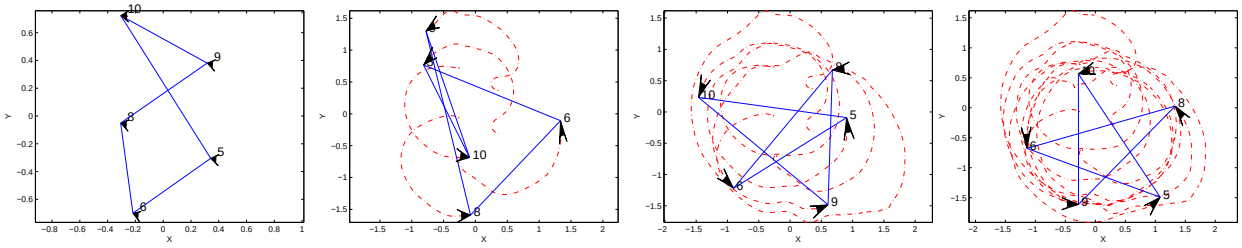

(a) (b) (c) (d)

Fig. 11. Five *Scarabs* form a circular formation starting with a ring topology while avoiding collisions. (a) $t = 0$ sec. (b) $t = 16$ sec. (c) $t = 40$ sec. (d) At $t = 80$ sec. the robots reach a stable balanced configuration, which is the star polygon $\{5/3\}$, around a circle with radius of 1m. Figures (a) through (d) show the actual trajectories of the robots and their connectivity graph at the times specified above.

comparison of the potential energies of the system with and without α_i term (22) are presented in Figure 9. The potential energy of the system is computed from $f = \sum_{i=1}^{n} f_i$ where f_i is given by (20). The peak in Fig. 9(a) corresponds to the configuration observed in Fig. 8(b) where robots become too close to each other. By using the control input (24) the potential energy of the 5-agent system monotonically decreases (see Fig. 9(b)) and the system stabilizes on a state that the potential energy of the entire system is minimized.

B. Circular Motion With Ring Topology

If every robot can only "sense" two other robots in the group, the topology of the connectivity graph will be a ring topology. Since the connectivity graph is assumed fixed, the agents need to be numbered during the experiments. For n even, the largest region of attraction is an $\{n/d\}$ polygon with $d = n/2$, which is not physically possible, because it requires that robots with even indices to stay on one side of a line segment and robots with odd indices to stay at the other side. For n odd, both simulations and experiment suggest that the largest region of attraction belong to star polygon $\{n/d\}$ with $d = (n \pm 1)/2$, therefore, there are only two possible ordering of the robots in the final circular formation. Figure 11 shows that in our experiment the robots are stabilized to the star polygon $\{5/3\}$.

Remark 2: When the communication graph is a fixed, directed graph with a ring topology, where agent i could only see agent $(i+1)/\mathrm{mod}(n)$, then the n-agent system would behave like a team of robots in cyclic pursuit [29].

C. Parallel Motion With Fixed Topology

The space limitations imposed by the ground truth verification system, prohibited us from testing the vision-based control law for parallel motion directly on Scarabs. However, the Player-Stage architecture system allowed us to generate simulations that were close to the real experiments. Figure 12 shows snapshots of the Gazebo simulation for a group of 5 *Scarabs*, each applying the vision-based control laws (18).

X. Conclusions and Future Work

We developed control laws for nonholonomic robots that only use simple visual measurements for reaching coordinated motions such as parallel and circular formations. The vision-based control laws were functions of quantities such as bearing, optical flow and time-to-collision, all of which could be measured from images. Only bearing measurements were needed for reaching a balanced circular formation, whereas for a parallel formation, additional measurements of optical flow and time-to-collision were required. We proved the local stability of the equilibria for both parallel and circular balanced formations, and verified the effectiveness of the theory though multi-robot experiments. In the end, collision avoidance properties were also added to the robots in order to obtain better results in the experiments. Note that when we work with robots that have limited field of view, directed connectivity graphs [23], [28] come into play. The study of motion coordination in the presence of directed communication graphs is the subject of an ongoing work.

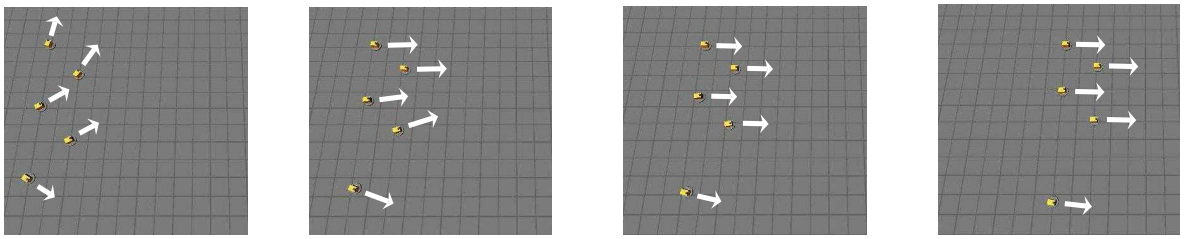

(a) t=0 sec. (b) t = 1 sec. (c) t=3 sec. (d) t=7 sec.

Fig. 12. Five *Scarabs*, starting with different initial orientations, apply the vision-based control input (18) to reach a parallel formation. The simulation is done in the simulator Gazebo.

XI. Appendices

A. Proof of Theorem 1

Assume an arbitrary orientation for the edges of graph $\mathcal{G} = (\mathcal{V}, \mathcal{E}, \mathcal{W})$. Consider the $n \times e$ incidence matrix, B, of this oriented graph with $n = |\mathcal{V}|$ vertices and $e = |\mathcal{E}|$ edges. Let $\boldsymbol{\theta} = [\theta_1 \dots \theta_n]^T$. Then, we can write (4) in the compact form as:

$$\dot{\boldsymbol{\theta}} = \boldsymbol{\omega} = \kappa B \sin(B^T \boldsymbol{\theta}), \quad \kappa < 0 \tag{25}$$

where $\sin(B^T\boldsymbol{\theta}) \in \mathbb{R}^e$ is a vector whose elements are $\sin(\theta_i - \theta_j)$. Equation (25) can be written in the form:

$$\dot{\boldsymbol{\theta}} = \boldsymbol{\omega} = \kappa B W(\theta) B^T \boldsymbol{\theta} = \kappa L_w(\boldsymbol{\theta})\boldsymbol{\theta}, \tag{26}$$

where $W(\boldsymbol{\theta}) = \text{diag}\{\text{sinc}(\theta_i - \theta_j) \mid (i,j) \in \mathcal{E}\}$ is a diagonal matrix whose entries are the edge weights for $\mathcal{G}$. The ordering of the elements on the diagonal of $W(\boldsymbol{\theta})$ is consistent with the ordering of the edges in the incidence matrix B. The matrix $L_w(\boldsymbol{\theta}) = BW(\boldsymbol{\theta})B^T$ can be thought of as the weighted Laplacian of $\mathcal{G}$, when $\text{sinc}(\theta_i - \theta_j) = \sin(\theta_i - \theta_j)/(\theta_i - \theta_j)$ is positive. A sufficient condition for this to hold is that $\boldsymbol{\theta}$ belongs to the open cube $(-\pi/2, \pi/2)^n$. In other words, over any compact subset of the cube $(-\pi/2, \pi/2)^n$, the dynamics can be represented by a state-dependent weighted Laplacian.

Now consider the Lyapunov function

$$s(\boldsymbol{\theta}) = \frac{1}{2}\sum_{j\sim i} |\mathbf{v}_i - \mathbf{v}_j|^2 = \sum_{j\sim i} 1 - \cos(\theta_i - \theta_j) \tag{27}$$

where the sum is over all the neighboring pairs, $i \sim j$. The above sum represents the total misalignment energy between velocity vectors. Since we have $s(\boldsymbol{\theta}) = e - \mathbf{1}^T \cos(B^T\boldsymbol{\theta})$, and because of (26), the time derivative of $s(\boldsymbol{\theta})$ along the trajectories of the system becomes

$$\dot{s} = \nabla s \; \dot{\boldsymbol{\theta}} = \boldsymbol{\theta}^T L_w \dot{\boldsymbol{\theta}} = (1/\kappa)\dot{\boldsymbol{\theta}}^T \dot{\boldsymbol{\theta}} \leq 0, \quad \kappa < 0 \; .$$

A simple application of LaSalle's invariance principle over the configuration space which is an n-torus and therefore compact reveals that all trajectories starting in anywhere on the n-torus converge to the largest invariant sets in $\{\theta \mid \dot{s}(\boldsymbol{\theta}) = 0\}$. Note that this is a very rich set and contains many equilibria other than the consensus set.

In order to prove that the consensus set is *locally attractive*, we utilize a simple quadratic Lyapunov function $v(\boldsymbol{\theta}) = \frac{1}{2}\boldsymbol{\theta}^T\boldsymbol{\theta}$, and the open cube $(-\pi/2, \pi/2)^n$. One can prove that any compact subset Ω of the open cube $(-\pi/2, \pi/2)^n$ is invariant. This can be easily seen by noting that any trajectory that approaches the boundary of the cube is pushed back to the interior of the cube by dynamics (4). Specifically, suppose θ_i is the first to approach the boundary of the cube. The term $\kappa \sin(\theta_i - \theta_j)$ is therefore negative for each $j \in \mathcal{N}_i$, therefore θ_i cannot push the boundary $\pi/2$. Similar argument can be made for the boundary $-\pi/2$.

Once the invariance of the cube is established, LaSalle's invariance principle can be used to show that the synchronized state is the only equilibrium within the set $\mathcal{M} = \{\boldsymbol{\theta} \in \Omega \mid \dot{v}(\boldsymbol{\theta}) = 0\}$, where Ω is a compact subset of cube $(-\pi/2, \pi/2)^n$. This is true since $\dot{v}(\boldsymbol{\theta}) = \kappa\boldsymbol{\theta}^T L_w \boldsymbol{\theta} \leq 0$ because $\kappa < 0$. Thus, equilibrium points are the set of solutions of $L_w\boldsymbol{\theta} = 0$. If graph $\mathcal{G}$ is connected, within Ω the null space of weighted Laplacian L_w is the span of vector $\mathbf{1}_n$. Thus, the solution is Null$\{L_w\}$, which is the set $\mathcal{S} = \{\boldsymbol{\theta} \mid \boldsymbol{\theta} \in \text{span}\{\mathbf{1}_n\}\}$. This suggests that all agents reach the same heading as $t \to \infty$.

B. Proof of Theorem 2

Let us define vector $\mathbf{p}$ that points towards the geometric center of the group:

$$\mathbf{p} = \frac{1}{n}\sum_{i=1}^{n} \mathbf{z}_i = \frac{1}{n}\mathbf{1}^T\mathbf{z} \; , \quad \mathbf{1} = \mathbf{1}_n \otimes I_2 \in \mathbb{R}^{2n\times 2} \; .$$

The minimum $|\mathbf{p}| = 0$ is reached when the position vectors $\mathbf{z}_i$ are in a balanced position (splay state); and the maximum $|\mathbf{p}| = 1$ is reached when all the position vectors are aligned (state synchronized). Note that the balancing input (6) can be bounded above by a function of vector $\mathbf{p}$:

$$\begin{aligned} u_i &= -\kappa \sum_{j\in\mathcal{N}_i} < \frac{\mathbf{z}_{ij}}{|\mathbf{z}_{ij}|}, \mathbf{v}_i > = -\kappa \sum_{j=1}^{n} \frac{1}{|\mathbf{z}_{ij}|} < \mathbf{z}_j, \mathbf{v}_i > \\ &\leq -\frac{\kappa}{|\mathbf{z}|_{max}} \sum_{j=1}^{n} < \mathbf{z}_j, \mathbf{v}_i > \\ &= -\frac{n\kappa}{|\mathbf{z}|_{max}} < \mathbf{p}, \mathbf{v}_i > \; , \quad \kappa > 0 \; , \end{aligned} \tag{28}$$

where $|\mathbf{z}|_{max} = \max\{|\mathbf{z}_{ij}|, \; (i,j) \in \mathcal{E}\}$, and we have used the fact that $\mathbf{v}_i \perp \mathbf{z}_i$.

Now consider the following Lyapunov function

$$w(\mathbf{z}) = \frac{n}{2}|\mathbf{p}|^2 = \frac{1}{2n}\mathbf{z}^T\mathbf{1}\mathbf{1}^T\mathbf{z} \tag{29}$$

which is minimized for the balanced formation. Given the gradient of $w(\mathbf{z})$:

$$\frac{\partial w(\mathbf{z})}{\partial \mathbf{z}_i} = \frac{1}{n}(\mathbf{1}\mathbf{1}^T\mathbf{z})_i = \frac{1}{n}\mathbf{1}^T\mathbf{z} = \mathbf{p}$$

the time derivative of $w(\mathbf{z})$ becomes

$$\begin{aligned} \dot{w}(\mathbf{z}) &= \sum_{i=1}^{n} < \frac{\partial w(\mathbf{z})}{\partial \mathbf{z}_i}, \dot{\mathbf{z}}_i >= \sum_{i=1}^{n} < \mathbf{p}, \mathbf{v}_i > u_i \\ &\leq -\frac{n\kappa}{|\mathbf{z}|_{max}} \sum_{i=1}^{n} < \mathbf{p}, \mathbf{v}_i >^2 \leq 0 \end{aligned} \tag{30}$$

where we have used (28).

A simple application of LaSalle's invariance principle over the configuration space which is an n-torus and therefore compact reveals that all trajectories starting in anywhere on the n-torus converge to the largest invariant sets in $\mathcal{M} = \{\mathbf{z} \mid \dot{w}(\mathbf{z}) = \mathbf{0}\}$. This set is characterized by $< \mathbf{p}, \mathbf{v}_i >= 0$, for all $i \in \{1, \ldots, n\}$. Therefore the equilibria are given by either $\mathbf{p} = \mathbf{0}$, or $\mathbf{p} \perp \mathbf{v}_i$ for all $i \in \{1, \ldots, n\}$. $\mathbf{p} = \mathbf{0}$ is the global minimum of $w(\mathbf{z})$ and is asymptotically stable. At the equilibrium we have $u_i = 0$ for all $i \in \{1, \ldots, n\}$ and as a result the geometric center remains fixed because $\dot{\mathbf{p}} = \sum_i u_i \mathbf{v}_i = \mathbf{0}$.

The critical points given by $\mathbf{p} \perp \mathbf{v}_i$ correspond to a set of configurations that m agents are at antipodal position from the other $n - m$ agents, where $1 \leq m < n/2$. The instability of these equilibria is proved by showing that if we perturb the system at those equilibria, the system moves away from them and $w(\mathbf{z})$ will be decreasing.

Remark 3: The Laplacian matrix of a complete graph equals to $L_c = I_n - (1/n)\mathbf{1}_n\mathbf{1}_n^T$. Thus, one can see that minimizing $w(\mathbf{z})$ in (29) is equivalent to maximizing $\mathbf{z}^T\bar{L}_c\mathbf{z}$ with $\bar{L}_c = L_c \otimes I_2$. The maximum is achieved when all the agents are evenly spaced around the circle.

C. Proof of Theorem 3

Let L_r be the Laplacian matrix of a graph with a ring topology, and $\bar{L}_r = L_r \otimes I_2$. Input (6) can be written in terms of the Laplacian of the connectivity graph:

$$\begin{aligned} u_i &= \kappa \sum_{j \in \mathcal{N}_i} \frac{1}{|\mathbf{z}_{ij}|} < \mathbf{z}_i - \mathbf{z}_j, \mathbf{v}_i > \\ &\geq \frac{\kappa}{|\mathbf{z}|_{max}} \sum_{j \in \mathcal{N}_i} < \mathbf{z}_i - \mathbf{z}_j, \mathbf{v}_i > \\ &= \frac{\kappa}{|\mathbf{z}|_{max}} < (\bar{L}_r\mathbf{z})_i, \mathbf{v}_i >, \quad \kappa > 0 \end{aligned} \tag{31}$$

where $(\bar{L}_r\mathbf{z})_i \in \mathbb{R}^2$ is the subvector of $\bar{L}_r\mathbf{z}$ associated with the i^{th} agent. Now consider the function

$$s(\mathbf{z}) = \frac{1}{2}\mathbf{z}^T\bar{L}_r\mathbf{z}$$

that is *maximized* for the balanced formation, and this maximum exists because $s(\mathbf{z})$ is bounded from above. Using the dynamics (5) and input (6) we have that

$$\begin{aligned} \dot{s}(\mathbf{z}) &= \sum_{i=1}^{n} < \frac{\partial s(\mathbf{z})}{\partial \mathbf{z}_i}, \dot{\mathbf{z}}_i >= \sum_{i=1}^{n} < (\bar{L}_r\mathbf{z})_i, \mathbf{v}_i > u_i \\ &\geq \frac{\kappa}{|\mathbf{z}|_{max}} \sum_{i=1}^{n} < (\bar{L}_r\mathbf{z})_i, \mathbf{v}_i >^2 \geq 0 \end{aligned} \tag{32}$$

Thus $s(\mathbf{z})$ monotonically increases along the trajectories of system (5) with input (6), and converges to equilibria corresponding to

$$< (\bar{L}_r\mathbf{z})_i, \mathbf{v}_i >= 0, \quad \forall i \in \{1, \ldots, n\} . \tag{33}$$

Let us characterize the set of equilibria given by (33). We represent the unit vector $\mathbf{z}_i$ in the rotating frame by $\mathbf{z}_i = [\cos\theta_i \ \ \sin\theta_i]^T$. Then $\mathbf{v}_i = [-\sin\theta_i \ \ \cos\theta_i]^T$, and (33) is equivalent to

$$\sum_{j \in \mathcal{N}_i} \sin(\theta_i - \theta_j) = 0, \quad \forall i \in \{1, \ldots, n\} . \tag{34}$$

Let $\boldsymbol{\theta} = [\theta_1, \ldots, \theta_n]^T$. Then (34) becomes

$$B \sin(B^T\boldsymbol{\theta}) = 0 , \tag{35}$$

where $B \in \mathbb{R}^{n \times e}$ is the incidence matrix of $\mathcal{G}^{ring}$. For $\mathcal{G}^{ring}$, $n = e$ and B is a circulant matrix that satisfies $B\mathbf{1}_e = \mathbf{0}$. Let $\boldsymbol{\phi} = B^T\boldsymbol{\theta}$. Then the equilibria of system (35) are characterized by

$$\sin\boldsymbol{\phi} = \alpha\mathbf{1}_e \tag{36}$$

$$\mathbf{1}_e^T\boldsymbol{\phi} = m\pi , \tag{37}$$

for some $\alpha \in \mathbb{R}$ and $m \in \mathbb{N}$. Vector $\boldsymbol{\phi}$ satisfies equation (36) iff $\phi_k = \{\phi_o, \pi - \phi_o\}$ for all $k \in \{1, \ldots, e\}$ and $\phi_o \in (0, 2\pi)$. Equation (37) is satisfied if $\phi_o = (m/e)\pi$.

Next we prove the (local) exponential stability of the relative equilibria, *i.e.,* the balanced state. For the proof of the exponential stability of the equilibrium $\boldsymbol{\phi} = \phi_o\mathbf{1}_e$ we consider the linearization of system (35) about ϕ_o. The Jacobian of system $\dot{\boldsymbol{\theta}} = \kappa B \sin(B^T\boldsymbol{\theta})$ at the equilibrium is

$$J = \kappa B \mathrm{diag}\big(\cos\phi_o\big) B^T = \kappa \cos\phi_o B B^T$$

where $\mathrm{diag}\big(\cos\phi_o\big)$ is an $e \times e$ matrix with $\cos\phi_o$ as its diagonal elements. Since $\kappa > 0$, the linearized system $\dot{\boldsymbol{\theta}} = J\boldsymbol{\theta}$ is exponentially stable if $\phi_o \in (\pi/2, 3\pi/2)$.

D. Proof of Theorem 4

Consider the following nonnegative function as a measure of the energy of the system

$$w(\mathbf{v}, \mathbf{r}) = \frac{-\kappa_1}{2} < \mathbf{v}, \bar{L}\mathbf{v} > + \kappa_p \sum_{i=1}^{n} f_i , \tag{38}$$

where $\kappa_1 < 0$, $\kappa_p > 0$ and $f_i = \sum_{j \in \mathcal{N}_i} f_{ij}$. The time derivative of $w(\mathbf{v}, \mathbf{r})$ becomes

$$\begin{aligned} \dot{w}(\mathbf{v}, \mathbf{r}) &= -\kappa_1 \sum_{i=1}^{n} < \dot{\mathbf{v}}_i, (\bar{L}\mathbf{v})_i > + \kappa_p \sum_{i=1}^{n} < \dot{\mathbf{v}}_i, \nabla_{\mathbf{r}_i} f_i > \\ &= -\sum_{i=1}^{n} \omega_i \Big(\kappa_1 < \mathbf{v}_i^{\perp}, (\bar{L}\mathbf{v})_i > \\ &+ \kappa_p < \mathbf{v}_i^{\perp}, \nabla_{\mathbf{r}_{ij}} f_i > \Big) = -\sum_{i=1}^{n} \omega_i^2 \leq 0 , \end{aligned}$$

where in the last equality we used the expression (23) for the input, ω_i. Now consider the compact region Ω over which the potential function $w(\mathbf{v}, \mathbf{r})$ is decreasing. By an application of the LaSalles' invariance principle, any trajectory of the system starting in Ω asymptotically converges to the largest invariant set given by $\dot{w}(\mathbf{v}, \mathbf{r}) = 0$. The equilibria are characterized by

$$< \mathbf{v}_i^{\perp}, (\bar{L}\mathbf{v})_i > \;=\; 0\ , \tag{39}$$

$$< \mathbf{v}_i^{\perp}, \nabla_{\mathbf{r}_{ij}} f_i > \;=\; 0\ . \tag{40}$$

From (39) it is concluded that $\bar{L}\mathbf{v} = \mathbf{0}$. For a connected graph this implies that $\mathbf{v} \in \text{span}\{\mathbf{1}\}$. From (40) all it can be inferred is that $(B \otimes I_2)[\nabla f_{ij}] = \mathbf{0}$, where $B \in \mathbb{R}^{n \times e}$ is the incidence matrix of $\mathcal{G}$, and $[\nabla f_{ij}] = [\dots\ (\nabla_{\mathbf{r}_{ij}} f_{ij})^T\ \dots]^T \in \mathbb{R}^{2e}$ is the stack vector of all the gradients. If B is full rank (*i.e.,* $\mathcal{G}$ is a tree), then (40) implies that $[\dots\ (\nabla_{\mathbf{r}_{ij}} f_{ij})^T\ \dots]^T = \mathbf{0}$, meaning that all the distances converge to the desired values. If B is rank deficient, then the system converges to a local minimum, *i.e.,* a configuration that potential energy of the system is minimized.

REFERENCES

[1] M. Batalin, G.S. Sukhatme, and M. Hattig. Mobile robot navigation using a sensor network. In *IEEE International Conference on Robotics and Automation*, pages 636–642, 2004.

[2] R. W. Beard and V. Stepanyan. Synchronization of information in distributed multiple vehicle coordinated control. In *Proceedings of IEEE Conference on Decision and Control*, December 2003.

[3] S.S. Beauchemin and J.L. Barron. The computation of optical flow. *ACM Computing Surveys*, 27:433–467, 1995.

[4] R. Cipolla and A. Blake. Surface orientation and time to contact from image divergence and deformation. In *Proc. Second European Conference on Computer Vision*, pages 187–202, 1992.

[5] J. Cortes, S. Martinez, T. Karatas, and F. Bullo. Coverage control for mobile sensing networks. *IEEE Transactions on Robotics and Automation*, 20(2):243–255, February 2004.

[6] I.D. Couzin, J. Krause, R. James, G.D. Ruxton, and N.R. Franks. Collective memory and spatial sorting in animal groups. *Journal of Theoretical Biology*, 218(1):111, 2002.

[7] A. Das, R. Fierro, V. Kumar, J. Ostrowski, J. Spletzer, and C. J. Taylor. Vision based formation control of multiple robots. *IEEE Trans. Robotics and Automation*, 19:813–825, 2002.

[8] J. Fredslund and M.J. Mataric. A general algorithm for robot formations using local sensing and minimal communication. *IEEE Trans. Robotics and Automation*, pages 837– 846, 2002.

[9] S. N. Fry, R. Sayaman, and M. H. Dickinson. The aerodynamics of free-flight maneuvers in drosophila. *Science*, 300:495–498, 2003.

[10] B. Gerkey, R.T. Vaughan, and A. Howard. The player/stage project: Tools for multi-robot and distributed sensor systems. In *Proc. of the Int. Conf. on Advanced Robotics*, pages 317–323, Portugal, June 2003.

[11] D. Prattichizzo G.L. Mariottini, G.J. Pappas and K. Daniilidis. Vision-based localization of leader-follower formations. In *Proceedings of the 44th IEEE Conference on Decision and Control*, pages 635– 640, December 2005.

[12] C. Godsil and G. Royle. *Algebraic Graph Theory*. Springer Graduate Texts in Mathematics # 207, New York, 2001.

[13] T. Hamel and R. Mahony. Visual servoing of an under-actuated dynamic rigid-body system: an image-based approach. *IEEE Transactions on Robotics and Automation,*, 18(2):187–198, April 2002.

[14] A. Jadbabaie, J. Lin, and A. S. Morse. Coordination of groups of mobile autonomous agents using nearest neighbor rules. *IEEE Transactions on Automatic Control*, 48(6):988–1001, June 2003.

[15] A. Jadbabaie, N. Motee, and M Barahona. On the stability of Kuramoto model of coupled nonlinear oscillators. In *Proceedings of the American Control Conference*, volume 5, pages 4296– 4301, July 2004.

[16] James Jeanne, Naomi Leonard, and Derek Paley. Colletive motion of ring-coupled planar particles. In *44th IEEE Conference on Decision and Control and 2005 European Control Conference*, pages 3929 – 3934, Seville, Spain, December 2005.

[17] E.W. Justh and P.S. Krishnaprasad. Simple control laws for uav formation flying. *Naval Research Laboratory Technical Report*, June 2002.

[18] E.W. Justh and P.S. Krishnaprasad. Natural frames and interacting particles in three dimensions. In *IEEE Conference on Decision and Control*, pages 2841 – 2846, December 2005.

[19] E. Klavins and D. E. Koditschek. Phase regulation of decentralized cyclic robotic systems. *International Journal of Robotics and Automation*, 21(3):257–275, 2002.

[20] J. J. Koenderink and A. J. van Doorn. How an ambulant observer can construct a model of the enviornment from the geometrical structure of the visual inflow. *Kybernetik*, 1977.

[21] Y. Kuramoto. *Cooperative Dynamics in Complex Physical Systems*. Springer, Berlin, 1989.

[22] D. N. Lee and P. E. Reddish. Plummeting gannets - a paradigm of ecological optics. *Nature*, 5830:293–294, 1981.

[23] Dongjun Lee and Mark Spong. Stable flocking of inertial agents on balanced communication graphs. In *American Control Conference*, 2006.

[24] H. Levine, E. Ben-Jacob, I. Cohen, and W.-J. Rappel. Swarming patterns in microorganisms: Some new modeling results. In *IEEE Conference on Decision and Control*, pages 5073 – 5077, December 2006.

[25] Zhiyun Lin, Mireille Brouke, and Bruce Francis. Local control strategies for groups of mobile autonomous agents. *IEEE Transactions on Automatic Control*, 49(4):622–629, April 2004.

[26] D. J. Low. Following the crowd. *Nature*, 407:465–466, 2000.

[27] W. MacFarland and S. Levin. Modeling the effects of current on prey aquisition in planktivorous fishes. *Mar. Fresh. Behav. Physiol.*, 35(1-2):69–85, 2002.

[28] J.A. Marshall and M.E. Broucke. On invariance of cyclic group symmetries in multiagent formations. In *Proceedings of 44th IEEE Conference on Decision and Control, and the European Control Conference*, pages 746– 751, Seville, Spain, December 2005.

[29] J.A. Marshall, M.E. Broucke, and B.A. Francis. Formations of vehicles in cyclic pursuit. *IEEE Transaction of Automatic Control*, 49:1963–1974, November 2004.

[30] N. Michael, J. Fink, and V. Kumar. Controlling a team of ground robots via an aerial robot. In *Proc. of the IEEE/RSJ Int. Conf. on Intelligent Robots and Systems*, San Diego, CA, November 2007.

[31] N. Moshtagh and A. Jadbabaie. Distributed geodesic control laws for flocking of nonholonomic agents. *IEEE Transaction on Automatic Control*, 52:681–686, April 2007.

[32] P. Ogren, E. Fiorelli, and N.E. Leonard. Cooperative control of mobile sensing networks: Adaptive gradient climbing in a distributed environment. *IEEE Transaction on Automatic Control*, 49(8):1292–1302, August 2004.

[33] A. Okubo. Dynamical aspects of animal grouping: swarms, schools, flocks, and herds. *Advances in Biophysics*, 22:1–94, 1986.

[34] R. Olfati-Saber. Flocking for multiagent dynamical systems: algorithms and theory. *IEEE Transactions on Automatic Control*, 51(3):401–420, March 2006.

[35] D. A. Paley, N. E. Leonard, R. Sepulchre, D. Grunbaum, and J. K. Parrish. Oscillator models and collective motion. *IEEE Control Systems Magazine*, 27(4):89 – 105, August 2007.

[36] M. Pavone and E. Frazzoli. Decentralized policies for geometric pattern formation and path coverage. *ASME Journal on Dynamic Systems, Measurement, and Control*, 2007.

[37] R. Sepulchre, D. Paley, and N Leonard. Stabilization of planar collective motion: All-to-all communication. *IEEE Transaction of Automatic Control*, 52(5):811 – 824, May 2007.

[38] S. H. Strogatz. From Kuramoto to Crawford: exploring the onset of synchronization in population sof coupled nonlinear oscillators. *Physica D*, 143:1–20, 2000.

[39] H. Tanner, A. Jadbabaie, and G. Pappas. Flocking in fixed and switching newtorks. *IEEE Transaction of Automatic Control*, 52:863–868, 2007.

[40] R. Vidal, O. Shakernia, and S. Sastry. Formation control of nonholonomic mobile robots with omnidirectional visual servoing and motion segmentation. In *IEEE International Conference on Robotics and Automation*, volume 1, pages 584 – 589, September 2003.

[41] W. Wang and J. J. E. Slotine. On partial contraction analysis for coupled nonlinear oscillators. *technical Report, Nonlinear Systems Laboratory, MIT*, 2003.

[42] Y. Wang and B.J. Frost. Time to collision is signalled by neurons in the nucleus rotundus of pigeons. *Nature*, 356(6366):236–238, 1992.

[43] Hong Zhang and James P. Ostrowski. Visual motion planning for mobile robots. *IEEE Transactions on Robotics and Automation*, 18(2):199 – 208, April 2002.